# Changes in 1958-2019 Greenland Surface Mass Balance are Attributable to both Greenhouse Gases and Anthropogenic Aerosols

Yan-Ning Kuo[1], Riley Culberg[1], and Flavio Lehner[1,2]

[1]Department of Earth and Atmospheric Sciences, Cornell University, Ithaca, NY, USA
[2]Polar Bears International, Bozeman, MT, USA

**Correspondence:** Yan-Ning Kuo (yk545@cornell.edu)

**Abstract.** Greenland Ice Sheet (GrIS) mass loss is a main contributor to rising Global Mean Sea Level (GMSL), exhibiting decadal variability due to surface mass balance (SMB) changes. Greenhouse gases (GHG) have long been identified as a key driver of GrIS mass loss through warming-induced runoff. However, there has not been a formal attribution of historical GrIS SMB changes to GHG and the potential role for other forcings such as anthropogenic aerosols (AAER). Here, we use the
5 Community Earth System Model version 2 large ensemble and single forcing large ensemble (CESM2-LE and CESM2-SFLE) to formulate a detection and attribution analysis for historical GrIS SMB changes. We show that the decadal variability of SMB is forced by historical radiative forcing attributable to both GHG and AAER through their forced changes of runoff. This highlights that, in addition to the frequently mentioned GHG, AAER also contributes to SMB changes during the historical period. GHG influences GrIS runoff mainly through long-term radiatively-forced warming, while AAER influences it through
10 the decadal variability of atmospheric circulation that projects onto a Greenland blocking pattern, leading to relative cooling from cyclonic circulation over Greenland pre-1980 and relative warming from anti-cyclonic circulation thereafter. The attribution of SMB, and specifically runoff, to AAER has a lower signal-to-noise ratio (S/N) than the attribution to GHG due to both a weaker signal and wider confidence intervals. The lower S/N in attributing runoff changes to AAER is partly due to a smaller temperature response in AAER than in GHG and partly due to a mean state temperature dependency of the runoff sensitivity.
15 In simulations with only AAER, the climate is colder than in simulations with all forcings or only GHG, leading to more time below freezing when temperature variations do not affect runoff as much. We resolve this issue by comparing simulations with all forcings with simulations in which everything-but-AAER is changing, thereby stressing the need to account for mean state dependencies when conducting detection and attribution with single forcing simulations.

## 1 Introduction

20 The global mean sea level (GMSL) has been rising at an averaged rate of 1.56 mm/year since 1900 (Frederikse et al., 2020; Hay et al., 2015; Church et al., 2011) and has accelerated to 3.3 mm/year since the 1990s (Chen et al., 2017; Church et al., 2011). A growing contribution to GMSL rise is from the ocean mass increase (barystatic sea level rise), due to freshwater input to the ocean from terrestrial water, mountain glaciers, and polar ice sheets, including both the Greenland Ice Sheet (GrIS) and Antarctic Ice Sheet. Glaciers remain the least constrained component of the climate change-driven sea level rise (IPCC AR6,

25  2023). Among these glacial GMSL sources, the GrIS is one of the largest barystatic sea level contributors to GMSL since
1900 (accounting for 29% of the total GMSL increase; Frederikse et al. 2020). Along with contributing to GMSL rise, GrIS
mass loss can further increase regional sea level rise rate, such as for the North American East Coast (Mitrovica et al., 2001),
resulting in higher risk of coastal flooding (Wdowinski et al., 2016).

GrIS mass loss comes from two factors (Mouginot et al., 2019): (1) changes in the surface mass balance (SMB), defined as
30  the difference between precipitation, evaporation/sublimation, and runoff, and (2) changes in ice discharge related to glacial
dynamics, manifested in calving trends. Observational records show that declining GrIS SMB has become an increasingly
important contributor to rising GMSL in recent decades (Enderlin et al., 2014; Kjeldsen et al., 2015; Mouginot et al., 2019)
and GrIS SMB change is identified as the largest source of GMSL uncertainty in future projections (Pattyn et al., 2018). Thus,
understanding why the SMB has changed historically can be informative for projecting future changes of GMSL due to GrIS
35  mass loss.

GrIS SMB reduction has been linked to rising air temperature over Greenland, as warming leads to more ice melting and
runoff (Trusel et al., 2018; van Kampenhout et al., 2020; Thompson-Munson et al., 2024). Greenhouse Gases (GHG) amplify
warming over the Arctic (Wu et al., 2024), and the consequent runoff increase is consistent with the monotonic long-term
decline in GrIS SMB projected for the future under strong radiative forcing scenarios (Hofer et al., 2020). However, there has
40  not been a formal attribution of historical GrIS SMB changes to radiative forcing, despite the emerging signal from GHG-
induced global mean temperature warming in recent decades (Deser et al., 2020a). The GrIS SMB decline since the 1990s
has also been linked to the increasing frequency of subsidence-induced warming from Greenland blocking, itself linked to
the negative phase of the North Atlantic Oscillation (NAO). NAO-related GrIS SMB change has thus far been treated as
internal variability on decadal time scales (Sherman et al., 2020; Brils et al., 2023; Hanna et al., 2022). However, new literature
45  attributes the negative NAO transition to anthropogenic aerosols (AAER; Dong and Sutton, 2021) and provides evidence of
AAER-forced historical decadal variability for different aspects of North Atlantic climate, including storm tracks (Kang et
al., 2024) and sea surface temperatures (SSTs; He et al., 2023). We hypothesize that internal variability might not be the only
reason for the recent decadal GrIS SMB changes; instead, both GHG and AAER could have also contributed.

Unlike GHG, historical AAER emissions had a non-monotonic spatio-temporal trajectory, owing to, for example, the timing
50  of social-economic development and air quality regulations in different countries (Persad et al., 2022). This heterogeneous
characteristic of AAER has been argued to induce historical decadal variability in various aspects of the Earth's climate;
prominent recent examples include tropical sea surface temperature (SST) patterns (Hwang et al., 2024; Dittus et al., 2021;
Takahashi and Watanabe, 2016), regional hydroclimate change (Kuo et al., 2023), and mid-latitude circulation (Dow et al.,
2021; Oudar et al., 2018). Together with the literature supporting AAER-forced historical decadal variability of North Atlantic
55  climate, we hypothesize that AAER contributes to GrIS SMB changes through its impacts on a circulation pattern projected
onto NAO.

However, the forced response to AAER often has a low signal-to-noise ratio (S/N; Dittus et al., 2021; Oudar et al., 2018;
Kuo et al., 2025), and so do externally forced NAO changes (McKenna and Maycock, 2021; Scaife and Smith, 2018). Different
external radiative forcings can also create nonlinear (or non-additive) responses in the climate system (Simpson et al., 2023;

60    Kuo et al., 2025). As such, nonlinear interactions between AAER and GHG forcings cannot be captured in the single forcing runs of AAER-only or GHG-only simulations. New climate model large ensembles are designed to better isolate subtle signals and responses to individual forcings from internal variability (Deser et al., 2020b). Therefore, in this study, we utilize the Community Earth System Model version 2 (CESM2; Danabasoglu et al., 2020) large ensemble (CESM2-LE; Rodgers et al., 2021) and its single forcing large ensemble (CESM2-SFLE) with both *forcing-only* and *all-but-forcing* experimental setups

65    (Simpson et al., 2023) to better understand whether the historical decadal variability of GrIS SMB is forced by both GHG and AAER.

       In this paper, we apply the detection and attribution (D&A) framework from Allen and Stott (2003) to formally assess whether historical radiative forcings can account for GrIS SMB changes between 1958-2019. We demonstrate that both GHG and AAER contributed to the 1958-2019 GrIS SMB changes and highlight a previously underappreciated source of uncertainty

70    in D&A when the climate response has mean state temperature dependency. This mean state temperature dependency can lead to different S/N for the attribution to GHG compared to AAER. Finally, we will discuss implications of these uncertainties for the general D&A framework.

## 2    Data and Methods

### 2.1    Data

75    #### 2.1.1    Reference data

In this study, reconstruction data, reanalysis data, and a regional climate model simulation driven by reanalysis since 1958 are included as reference data for the historical period. Frederikse et al. (2020)'s reconstruction for GrIS mass loss was used to assess the impact of SMB change on GrIS GMSL contributions since 1958. The Frederikse et al. (2020)'s reconstruction data comes from a Monte Carlo simulation perturbing the known prior estimate based on three estimates of GrIS mass loss

80    data, including a reconstruction from geological inference of historical ice sheet surface elevation (Kjeldsen et al., 2015), an input-output estimate (Mouginot et al., 2019), and a synthesis of satellite observations with a multi-method assessment (Bamber et al., 2018). With 5000 ensemble members, this reconstruction provides a range of observational uncertainty of the GMSL contribution from GrIS mass loss. To understand the drivers of the GrIS GMSL contribution, we use annual mean SMB, precipitation (P), and runoff (R), averaged over the GrIS, from the polar regional climate model RACMO2.3p2, ran

85    at 5.5 km resolution and statistically downscaled to 1km, and forced with the reanalysis data sets from ECMWF Reanalysis (ERA), hereafter RACMO-ERA (Noël et al., 2022), for 1958-2019. This RACMO-ERA simulation has been compared against in-situ meteorological data and point measurements of GrIS SMB and showed good agreement with these observations (Noël et al., 2018). Here, these RACMO-ERA outputs are treated as the reference data to formulate a D&A analysis. Additionally, annual means of near-surface temperature at 2m (TAS) and 500 hPa geopotential height (Z500) from monthly gridded ERA5

90    reanalysis (Hersbach et al., 2020) are included to investigate the atmospheric drivers of the SMB changes.

### 2.1.2 CESM2 large ensemble and single forcing large ensemble (CESM2-LE and CESM2-SFLE)

CESM2-LE and CESM2-SFLE are used for the D&A analysis. CESM2 (Danabasoglu et al., 2020) is a climate model developed by the National Center for Atmospheric Research (NCAR). It includes a land ice model (CISM; Lipscomb et al., 2019) of the GrIS at 4 km spatial resolution. CESM2-LE and CESM2-SFLE are run under compsets with a fixed ice sheet topography so that CISM does not feed back to other parts of the climate system but provides the finer grids to downscale SMB. CESM2 has been evaluated against observations and shown to capture the variability of GrIS SMB well (van Kampenhout et al., 2020; Noël et al., 2020; Noël et al., 2022).

We take the 50-member ensemble from CESM2-LE (Rodgers et al., 2021) that is forced with the full historical radiative forcings (ALL), using smoothed biomass burning forcing (*smbb*). Each ensemble member differs from the others due to initial condition perturbations (see Rodgers et al., 2021) to quantify the uncertainty originating from internal variability. CESM2-SFLE (Simpson et al., 2023) uses the same CESM2 version but instead of the ALL forcing, individual forcings are applied in isolation. We use the 15-member GHG and AAER simulations, as GHG and AAER are two dominant anthropogenic forcings for historical climate change. In CESM2-SFLE, the GHG (AAER) simulation is forced with time-evolving GHG (AAER) forcing, with other forcing held fixed at 1850 levels (i.e., the *forcing-only* experimental setup). We also include the 10-member all-but-aerosols (xAAER; the *all-but-forcing* experimental setup) simulations and follow Deser et al. (2020a) to calculate the contribution of anthropogenic aerosols as the difference between ALL and xAAER (ALL-minus-xAAER). With xAAER and ALL-minus-xAAER, we can assess the robustness of D&A results given the potential non-additivity issue reported in Simpson et al. (2023).

We use the annual SMB, and monthly P, R, TAS, and Z500 from these simulations. Monthly CESM2 outputs are converted to an annual sum (P, R) or annual mean (TAS, PSL) to compare against annual SMB. The area-weighted SMB, P, R (unit: mm per year) is summed over Greenland and divided by the global ocean area derived from the CESM2 land mask to convert into a GMSL equivalent (unit: mm GMSL equivalent per year). This GMSL equivalent is multiplied by 361.8 to convert to Gt per year. Anomalies are calculated by removing the 1958-2019 climatological means for regression analyses.

## 2.2 Detection and attribution (D&A) approach

D&A is commonly performed with a regression of the observation ($y$) onto the fingerprint(s) of the external forcing ($x_i$) as

$$y = \sum_{i=1}^{m} \beta_i x_i + \epsilon_y \tag{1}$$

where $\beta_i$ is the scaling factor(s) to best match the time-dependent fingerprint(s) to the observation, the fingerprint(s) $x_i$ are usually estimated by averaging many simulations (e.g., ensemble mean), and $\epsilon_y$ is the residual not explained by the simulated forced response (e.g., internal variability)(Allen and Scott, 2003; Swart et al., 2018). In this paper, we treat the RACMO-ERA simulation as $y$ as there is no in-situ observation of GrIS SMB at the temporal and spatial coverages necessary for this D&A analysis; $x_i$ are estimated by ensemble mean of CESM2-LE and CESM2-SFLE. For the univariate case ($i = 1$), $x_i$ is estimated

by the ensemble mean from ALL as $x_{ALL}$; for the bivariate case ($i = 2$), $x_i$ are estimated by the ensemble mean from GHG and AAER as $x_{GHG}$ and $x_{AAER}$ (or $x_{xAAER}$ and $x_{ALL-minus-xAAER}$). Eq. (1) can be solved by performing an ordinary least squares (OLS) regression with $y$ and $x_i$. In this case, we assume $x_i$ is observed without uncertainty. When $\beta_i$ is significantly

125 larger than 0, the forced response from fingerprint(s) $x_i$ is considered detectable; when $\beta_i$ is not significantly different from 1, the forced response is considered attributable to the fingerprint(s) $x_i$. The significance level of $\beta_i$ is usually determined from the distribution of $\beta_i$ due to internal variability, estimated from climate models (e.g., from pre-industrial simulations (*PiControl*) or historical simulations from which the ensemble mean has been removed), and follows the IPCC guidance to indicate the significance of $\beta_i$ and the confidence of attributing this signal to a given forcing(s).

130 In practice, $x_i$ contains uncertainties, such as from the choice of climate models and the errors due to averaging over a finite number of ensemble members. A total least square (TLS) regression is a common solution to perform D&A to account for uncertainty in $x_i$ (Allen and Scott 2003; Kirchmeier-Young et al., 2017; Schurer et al., 2013). Eq. (1) can be rewritten as

$$y = \sum_{i=1}^{m} \beta_i (x_i - \epsilon_{x_i}) + \epsilon_y \tag{2}$$

where now, $\epsilon_{x_i}$ is introduced to account for the uncertainties in simulated forced response in $x_i$. A singular value decompo-

135 sition (SVD) on the system of equations can solve $\beta_i$ in a deterministic way for the TLS regression (Allen and Scott, 2003).

The choice of whether to use an OLS or TLS regression should be made with caution, as TLS regression is not necessarily preferred over OLS for climate change D&A (McKitrick 2023). For example, the deterministic solutions of TLS regression can be considered as a linear transformation of OLS regression coefficients and, mathematically, such a transformation could introduce an upward bias for the regression coefficients, leading to a potential false positive in D&A when determining $\beta_i$

140 with TLS regression (McKitrick 2023). Moreover, climate models have biases in simulating the internal variability, either too large or too small a magnitude, which makes estimating the significance level of $\beta_i$ from internal variability based on that from climate models an imperfect approach.

In this study, we instead construct a Bayesian TLS regression to reduce bias and account for the uncertainty from using a climate model large ensemble from a single model (CESM2-LE and CESM2-SFLE). We first construct an ensemble of

145 numerical experiments for an ideal case of one-dimensional linear regression $y = \beta x$ where both sampled data $y$ and $x$ have noise (see Supplementary Information). This experiment confirms that the deterministic TLS regression solution overestimates the regression coefficients when compared with OLS regression and that our Bayesian TLS regression can alleviate this upward bias (Figure S1). We also calculate the scaling factor for attributing GrIS SMB changes to ALL historical forcings with CESM2-LE with a deterministic OLS regression, a deterministic TLS regression, and a Bayesian TLS regression (Figure S2). Our results

150 demonstrate that our Bayesian TLS regression provides the most conservative estimate of the significance level of $\beta_i$ and does not overestimate the scaling factor in the same way as the deterministic TLS solution (Figure S2).

### 2.2.1 Bayesian TLS regression

A Bayesian TLS regression with a Markov Chain Monte Carlo (MCMC) technique is used to address concerns of using a deterministic TLS regression for D&A (Katzfuss et al., 2017). With prior knowledge about the data and the uncertainty it might introduce for the D&A analysis, we define three parameters to set up the Bayesian TLS regression: the scaling factors ($\beta_i$), the uncertainty of estimating the true forced response with CESM2-LE and CESM2-SFLE ($\sigma_x$), and the uncertainty of observing the true forced response in the reference data (i.e., usually due to internal variability; $\sigma_y$). With a Bayesian TLS regression, the parameters in a regression model ($\beta_i$, $\sigma_x$, $\sigma_y$) are estimated in a probabilistic way, with the priors of their distributions determined from the data from RACMO-ERA, CESM2-LE, and CESM2-SFLE. In addition, a latent variable, $x_{latent} \sim \mathcal{N}(x, \sigma_x^2)$, is introduced to represent an unknown true forced response(s) from CESM2-LE/CESM2-SFLE (i.e., $x_{latent}$, the true unknown fingerprint(s), is a draw from a normal distribution with mean determined by $x$ with a spread of $\sigma_x$). Therefore, we formulate the D&A with

$$x_{latent} \sim \mathcal{N}\left(x_{ensmean}, \left(\frac{\sigma_{x_{ensmean}}}{\sqrt{n}}\right)^2\right) \tag{3}$$

The mean of $x_{latent}$ is estimated by the ensemble mean from the simulation(s) used for D&A ($x_{ensmean}$) with a spread defined as the standard error of the estimated forced response from that ensemble mean ($\frac{\sigma_{x_{ensmean}}}{\sqrt{n}}$), where $n$ is the number of ensemble members. With the assumption of the posterior distribution of $y$ as

$$y \sim \mathcal{N}(\beta x_{latent}, \sigma_y^2) \tag{4}$$

the Bayesian TLS regression coefficient ($\beta_i$) is solved with PyMC. Technical details (including the setup for priors) and idealized numerical experiments can be found in the Supplementary Information.

In this paper, we use the Bayesian TLS regression to obtain 10,000 posterior samples of $\beta_i$ so that we can estimate the confidence level of the attribution based on the posterior distributions of $\beta_i$. This Bayesian TLS regression is also applied to estimate the temperature sensitivity of SMB and R to TAS in the reference data and the forced responses simulated by CESM2 (see Table S1 for setups of priors).

## 3 Results

### 3.1 Decadal variability in GMSL due to GrIS SMB changes

Reconstruction data from Frederikse et al., (2020) shows that total GrIS mass loss has decadal variability and this decadal variability comes from the anomalous SMB relative to its long-term climatology (Figure 1; correlation coefficient between SMB and total mass loss is 0.72, $p < 0.01$, at interannual time scales; 0.92, $p < 0.01$, for 10-year running means with effective degree of freedom, eDOF, reduced to 6). For example, there are positive SMB anomalies during 1970-2000, slowing the rise
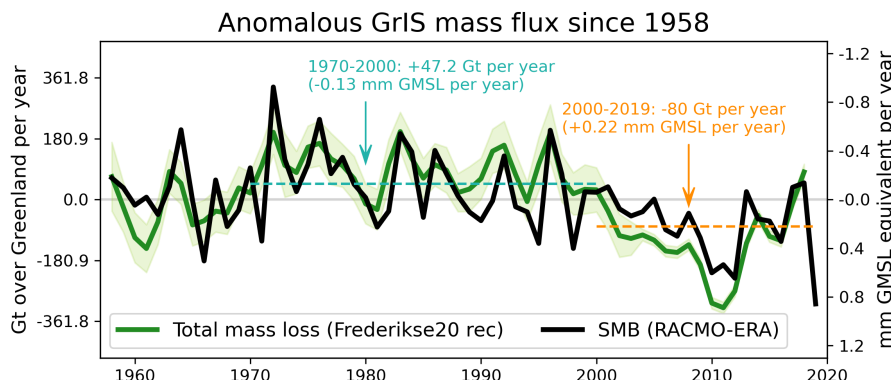
**Figure 1.** Decadal variability in GrIS' contribution to Global Mean Sea Level (GMSL) is observable and explained by decadal variability in surface mass balance (SMB). The anomalous (long-term mean subtracted) annual mass loss from GrIS Frederikse et al., (2020) reconstruction (green) and the anomalous annual GrIS SMB simulated by RACMO with ERA5 reanalysis (RACMO-ERA; black). The thick green lines are the 5000-member ensemble mean values of Frederikse et al. (2020) reconstruction, and the shadings are ±1 standard deviation across the 5000 ensemble members.

180 in GMSL due to GrIS mass loss (Figure 1); in turn, the greater decline in SMB after 2000 leads to an accelerated rise in GMSL contributed by GrIS. We note that the high correlations between the total mass loss from Frederikse et al. (2020) and the RACMO-simulated SMB reported here could also be influenced by the fact that reconstructed GrIS mass loss data usually includes RACMO-simulated SMB.

### 3.2 Detection and attribution of historical GrIS SMB changes

185 CESM2-LE with historical forcing (ALL) simulates a decline in SMB that is most apparent after 1990 (Figure 2a), despite a wide range of internal variability (purple shading) that also covers the interannual variability in RACMO-ERA. According to the D&A framework, the SMB change in RACMO-ERA is detectable and attributable to historical forcing with 99% confidence (i.e., *virtually certain*; Figure 2b). SMB changes can be approximated as precipitation (P) minus runoff (R; Figure S3, temporal correlation coefficient 0.99, *p < 0.01*, and 1.00, *p < 0.01*, for 10-year running mean time series with 6 eDOF), as sublimation

190 contributes <10% of SMB budget (van Kampenhout et al., 2020). The individual time series show that both ALL-forced precipitation and runoff increases (Figure 2c, 2e; note that R is inverted). However, this ALL-forced increase in precipitation is not detected in the observation (Figure 2d), meaning the observed variability of precipitation could just be internal variability (see also van Kampenhout et al., 2020). On the other hand, the increase in R is detectable and attributable to ALL historical forcing (Figure 2f; 99% confidence, *virtually certain*), agreeing with previous studies that historical GrIS SMB loss is mainly

195 due to warming-driven runoff changes (Noël et al., 2020; Noël et al., 2019; van Kampenhout et al., 2020).

The GrIS SMB changes from ALL (Figure 2a purple solid line) can be approximated as the sum of the changes from GHG and AAER (Figure S3; temporal correlation coefficient 0.66, *p < 0.01*, for SMB time series from ALL vs GHG+AAER
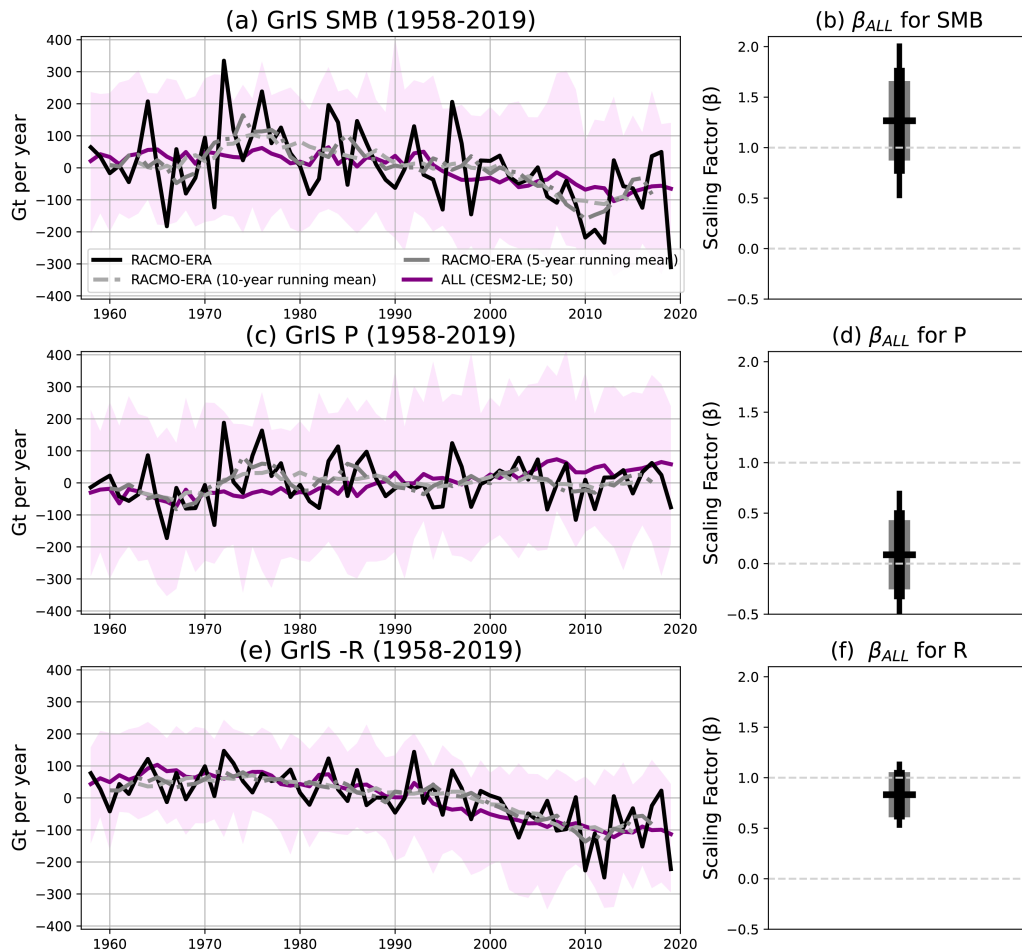
**Figure 2.** (a, c, e) Time series of GrIS SMB, P, -R since 1958 from RACMO-ERA (black; light gray and gray dashed lines are 10-year and 5-year running mean) and ensemble mean of CESM2-LE (purple). The purple shadings are the full range across ensemble members (i.e., maxima to minima). (b, d, f) Univariate scaling factors ($\beta_{ALL}$) of GrIS SMB, P, R. The horizontal line is the mean of the 10,000 posterior samples of $\beta_{ALL}$, and the gray shading/thick black vertical line/thin black vertical line is $\pm 1/ \pm 1.64/ \pm 2.57$ standard deviation of the 10,000 posterior samples of $\beta_{ALL}$, indicating the 66%/90%/99% confidence intervals in D&A (*likely/very likely/virtually certain* based on IPCC guideline).

and 0.93, *p < 0.01*, for 10-year running means with 6 eDOF), with GHG driving a long-term decline in SMB and AAER contributing to an increase before mid-1980 and a slight decrease thereafter (Figure 3a). Before mid-1980, GHG and AAER

200    basically cancel each other out, while they combine to drive the decline of ALL-forced SMB afterward (Fig. 3a).

     A bivariate Bayesian TLS regression is formulated to assess the D&A for these two historical radiative forcings, showing that both GHG (99% confidence, *virtually certain*) and AAER (90% confidence, *very likely*) contribute to the GrIS SMB changes (Figure 3b). Interestingly, the posterior distribution of $\beta_{GHG}$ has a narrower spread than the posterior distribution of $\beta_{AAER}$, implying a lower S/N in detecting the AAER-forced signal in RACMO-ERA SMB changes. Consistent with Figure 2, there

205    is no detectable precipitation change due to neither GHG nor AAER in RACMO-ERA (Figure 3c, 3d). However, there is a detectable GrIS runoff change attributed to both GHG and AAER, but both their influences are potentially underestimated (i.e., $\beta_{GHG}$ and $\beta_{AAER}$ are both significantly larger than 1), and $\beta_{AAER}$ also has a wider spread in its posterior distribution than $\beta_{GHG}$ for runoff (Figure 3e, 3f).

     Studies have shown that CESM2 has nonlinear forced responses due to different climate mean states (Simpson et al., 2023)

210    or the non-additive responses to different forcings (Kuo et al., 2025). Therefore, we repeat the bivariate D&A with SMB, precipitation, and runoff from the xAAER and ALL-minus-xAAER simulations to check the robustness of attributing both anthropogenic aerosols and greenhouse gases when using a climate model (CESM2) with reported nonlinear forced responses. Using xAAER and ALL-minus-xAAER to represent GHG and AAER forcing, this analysis yields robust conclusions: GHG and AAER create forced signals in the historical 1958-2019 GrIS SMB through runoff changes, and the attribution to both

215    xAAER and ALL-minus-xAAER is *virtually certain* (99% confidence; Figure S4). Interestingly, the posterior distribution of $\beta_{ALL-minus-xAAER}$ has a narrower spread for both SMB and runoff compared with the posterior distribution of $\beta_{AAER}$ (Figure S4b and Figure 3b for SMB and Figure S4f and Figure 3f for runoff), though $\beta_{ALL-minus-xAAER}$ and $\beta_{AAER}$ still have a wider spread than $\beta_{xAAER}$ and $\beta_{GHG}$. Additionally, runoff changes are not underestimated in ALL-minus-xAAER and xAAER (Figure S4f) as they are in GHG and AAER (Figure 3f), as the means of the posterior bivariate scaling factors are now

220    closer to (1,1). Thus, there appears to be a state dependence of the attribution to AAER.

     Overall, our D&A results indicate that historical GrIS SMB changes are attributable to both GHG and AAER through runoff changes. Despite differences in the scaling factors, these attribution results are robust to the sets of single forcing simulations used (*all-but-forcing* or *forcing-only* experimental setups with CESM2). We also point out there is a lower S/N when attributing GrIS SMB changes and runoff changes to AAER compared with attributing to GHG. This lower S/N when attributing to AAER

225    appears in two ways: (1) underestimated response ($\beta_{AAER} > 1$ and also $> \beta_{GHG}$) and (2) wider confidence intervals of $\beta_{AAER}$ than that of $\beta_{GHG}$.

### 3.3   Mean state temperature affects uncertainty in D&A for AAER

GrIS SMB has a stronger sensitivity to warming than to cooling (Thompson-Munson et al., 2024), and runoff has a nonlinear relationship to temperature change (Trusel et al., 2018). This nonlinear runoff response to temperature is commonly seen in

230    cryospheric variables in response to different mean state temperatures (Gottlieb and Mankin 2024) with different energy barrier to overcome and/or different positive degree days to start melting and inducing runoff changes (Sherman et al., 2020). Here, we
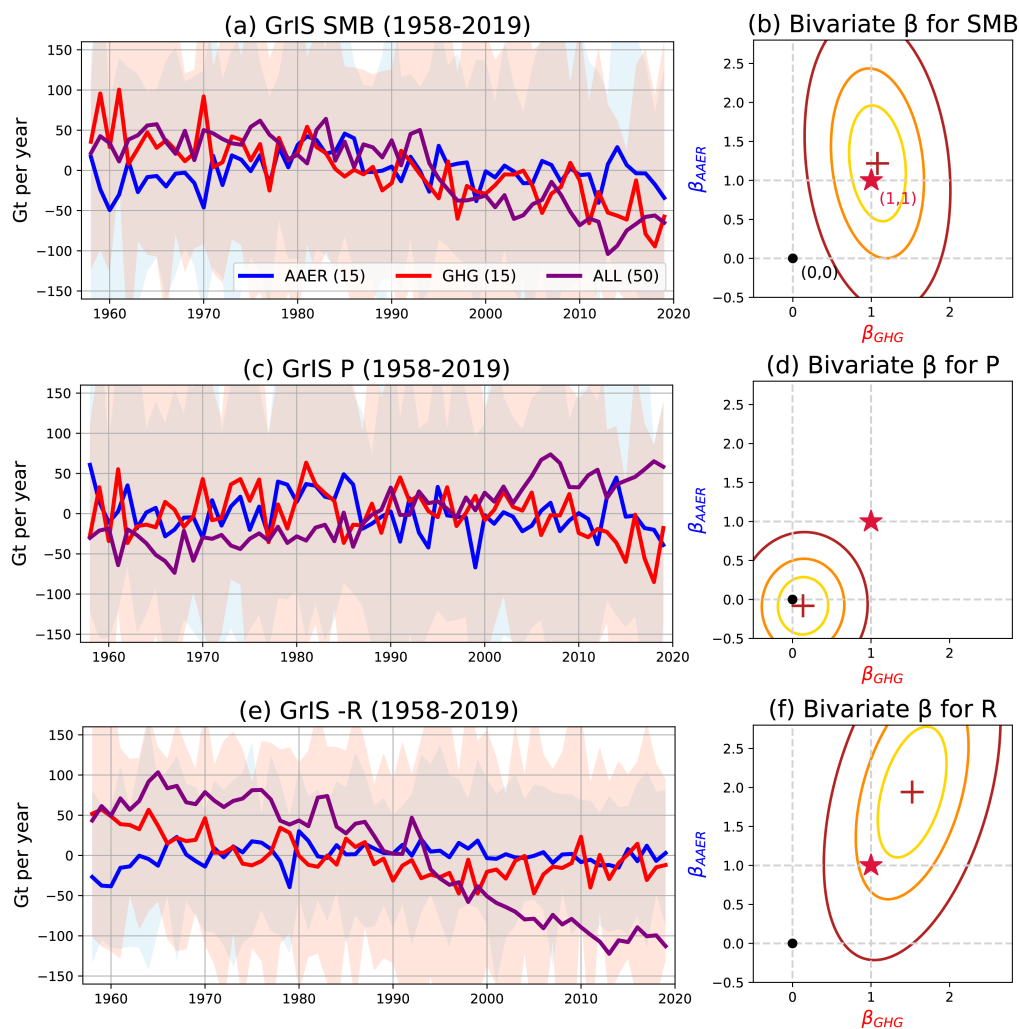
**Figure 3.** (a, c, e) Time series of GrIS SMB, P, -R since 1958 from ensemble mean of CESM2-SFLE greenhouse gases-only simulation (GHG; red), ensemble mean of CESM2-SFLE anthropogenic aerosols-only simulation (AAER; blue), ensemble mean of CESM2-LE ALL simulation (purple as Figure 2). The red/blue shadings are the full range across ensemble members (i.e., maxima to minima) in GHG/AAER. (b, d, f) Bivariate scaling factors ($\beta_{GHG}$ and $\beta_{AAER}$) of GrIS SMB, P, R. The firebrick plus symbol is the mean of the 10,000 posterior samples of $\beta_{GHG}$ and $\beta_{AAER}$, and the golden/orange/firebrick confidence ellipses are the 66%/90%/99% confidence intervals in $\beta_{GHG}$ and $\beta_{AAER}$ for D&A (likely/very likely/virtually certain based on IPCC guideline). When the confidence ellipse includes the point (1,1) (shown as the crimson star) and excludes the origin (0,0) (shown as the black dot), a bivariate attribution to both forcings is established.
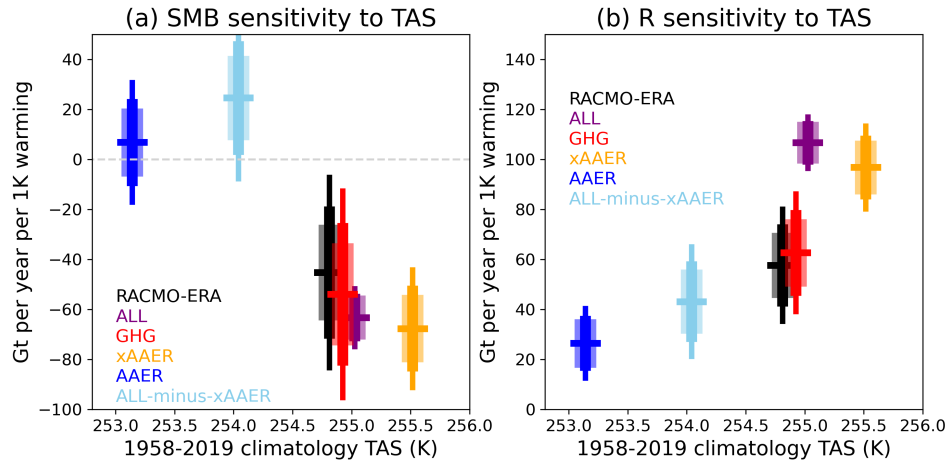
**Figure 4.** (a) The observed (RACMO-ERA; black) and forced (ALL, GHG, xAAER, AAER, ALL-minus-xAAER; purple, red, orange, blue, light blue respectively) GrIS SMB sensitivity to near-surface temperature during 1958-2019 sorted by the climatological mean near-surface temperature. (b) The observed (RACMO-ERA; black) and forced (ALL, GHG, AAER; purple, red, blue, light blue respectively) GrIS R sensitivity to near-surface temperature during 1958-2019 sorted by the climatological mean near-surface temperature.

hypothesize that the different temperature sensitivities of runoff in these different simulations might contribute to the lower S/N of the attribution to AAER compared with the attribution to GHG. SMB has a negative temperature sensitivity in RACMO-ERA, ALL, and GHG simulations (Figure 4a), and all of these simulations demonstrate apparent increases in runoff with

235  warming (Figure 4b). However, this negative temperature sensitivity is not seen in the AAER simulation (Figure 4a). There is a nonlinear temperature sensitivity of runoff if the simulations are sorted by their 1958-2019 climatological temperatures (Figure 4b), explaining the lack of negative temperature sensitivity of SMB in AAER (Figure 4a). In addition, the mean temperature over GrIS has a weaker forced response in AAER (ALL-minus-xAAER) than in GHG (xAAER) (Figure S5). Together with the weaker temperature sensitivity of SMB in AAER due to the weaker temperature sensitivity of runoff, these two factors lead

240  to a generally lower S/N in attributing SMB changes to AAER than GHG.

This mean state temperature dependent SMB and runoff sensitivity can also explain why the uncertainty ellipse of $\beta$ using xAAER and ALL-minus-xAAER (Figure S4) is smaller than the uncertainty ellipse using AAER and GHG (Figure 3). This is because xAAER and ALL-minus-xAAER simulations both have higher mean state temperatures than AAER and GHG simulations (orange vs red bars and light blue vs blue bars in Figure 4). The runoff responses are thus stronger in both the

245  xAAER and ALL-minus-xAAER simulations, and therefore easier to detect; $\beta_{xAAER}$ and $\beta_{ALL-minus-xAAER}$ are both closer to (1,1) with narrower posterior distributions (Figure 3f vs Figure S4f). Although the attribution to AAER is robust across *all-but-forcing* or *forcing-only* experimental setups in CESM2, these results demonstrate that mean state temperatures in different simulations can affect their runoff responses and therefore our confidence in attributing SMB changes to that forcing with this D&A framework.

## 3.4 Atmospheric drivers of forced GrIS runoff changes

What are the mechanisms by which GHG and AAER forcing drive long-term trends and decadal variability in GrIS SMB through runoff changes? Here, we focus on the summer (JJA) temperature and circulation patterns to explain the GrIS runoff changes, which are linked to the melting-induced runoff changes (Sherman et al., 2020; Hanna et al., 2014; Tedesco and Fettweis 2020). The trend map for 1958-2019 from ERA5 shows overall JJA polar warming and increasing Z500 over Greenland (Figure 5a), consistent with the Greenland Block Index (GBI) time series (Fig. S6). JJA near-surface warming and increased Z500 over the North Atlantic sector are visible in both ALL (Figure 5b) and GHG (Figure 5c). However, in GHG, the Atlantic Meridional Overturning Circulation (AMOC) declines more rapidly than in ALL, as it lacks the offsetting North Atlantic cooling from AAER (Figure 9 in Simpson et al., 2023), leading to cooling in the Subpolar Gyre. Additionally, ALL-forced JJA Z500 increases with a blocking-like structure over Greenland, while GHG-forced JJA Z500 increases more uniformly (Figure 5b vs Figure 5c contour). A cooling of the Subpolar Gyre in GHG simulation and a stronger subsidence trend in ALL together lead to *less* warming in GHG than in ALL (Figure 5b vs 5c).

Though the ALL-forced Z500 is weaker than the observed Z500 trend (consistent with GBI in Figure S6 and Delhasse et al. (2020)), the observed trend is within the range of possible trends from the 50-member ALL ensemble. The forced temperature and Z500 trends from ALL and GHG are overall alike, confirming that GHG contributes to the long-term linear trend seen in these atmospheric variables related to GrIS runoff changes. AAER, on the other hand, contributes almost nothing to this long-term trend pattern (Figure 5a vs 5d). These trend maps imply that the detected signal from AAER during 1958-2019 (Figure 3b, 3f) does not arise through the long-term linear trend but through forced decadal variability undergoing phase changes during this time period.

We compare maps of the correlation between annual GrIS runoff and JJA near-surface temperature and JJA Z500 from ERA5 (Figure 5e) and from the ensemble mean of AAER during 1958-2019 (Figure 5f). The AAER-based correlation map shows a pattern that is distinct from its long-term trend (Figure 5f vs Figure 5d); instead, the correlation map shows a pattern more similar to the ERA5-based correlation map (Figure 5e vs 5f). Both ERA5 and AAER have positive correlations between GrIS runoff and near-surface temperature and Z500, and the correlation pattern in ERA5 remains consistent even after detrending and temporal smoothing (Figure S7). Thus, the correlation pattern in ERA5 is mostly independent of the long-term linear trend. The correlation pattern in ERA5 shows a blocking over Greenland, which provides more cloudless days and subsidence-induced warming (Sherman et al., 2020), as well as warm air advection towards Western Greenland (Hanna et al., 2014; Tedesco and Fettweis 2020) due to the anti-cyclone over Greenland. Figure 5f confirms a similar correlation pattern due to AAER, supporting an AAER-forced change in the variability of circulation, imprinted onto a pattern that reinforces Greenland blocking.

## 4 Discussion and Conclusion

In this paper, we formulate a D&A analysis with CESM2-LE and CESM2-SFLE to investigate 1958-2019 GrIS SMB change and show that the historical SMB change is attributable not only to GHG but also to AAER. To our knowledge, this is the first
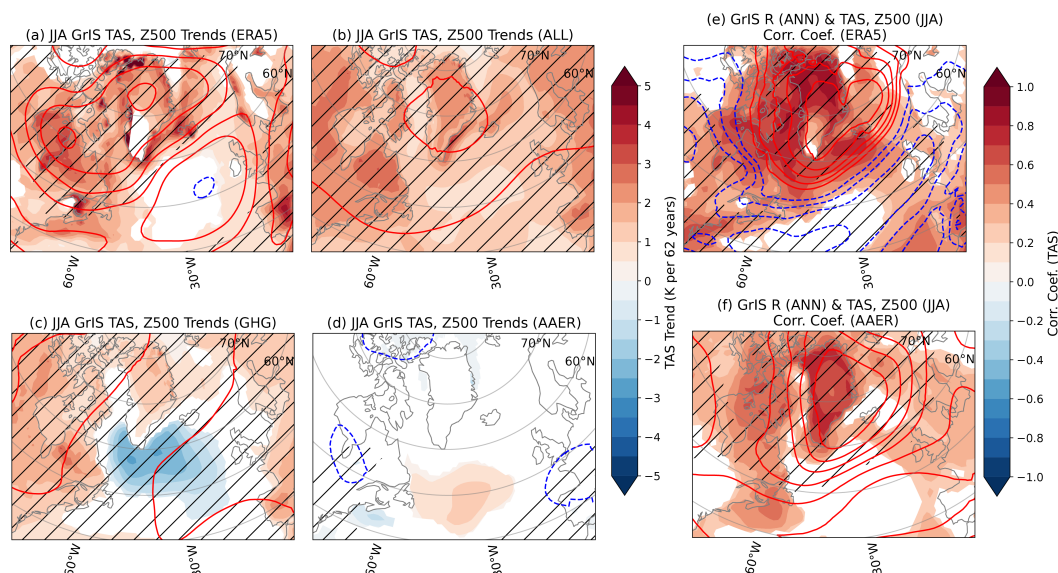
**Figure 5.** Trend maps of 500 hPa geopotential height (Z500; contours) and near-surface air temperature (TAS; shading) during 1958-2019 in (a) ERA5 reanalysis, (b) ensemble mean of all forcings CESM2-LE simulation (50; ALL), (c) ensemble mean of GHG-only simulation (15; GHG), and (d) ensemble mean of AAER-only simulation (15; AAER). Grid cells with insignificant TAS trends are masked out (95% confidence for ERA5, and ensemble mean trend over 1 standard deviation across all trends in the ensemble for climate model simulations). Grid cells with significant Z500 trends are hatched (95% confidence for ERA5 and ensemble mean trend over 1 standard deviation across all possible trends in the ensemble for climate model simulations). Z500 contours start from ±10 (m per 62 years) with contour spacings 10 (m per 62 years). (e-f) Correlation map of GrIS R with Z500 (contours) and TAS (shading) during 1958-2019 in (e) ERA5 reanalysis and (f) 15-member mean AAER. Insignificant TAS correlations are masked out and significant Z500 correlations are hatched (95% confidence). Contours start from 0.1 with contour spacings 0.1. The significance level of the correlation coefficients is based on a *t-test* with the degrees of freedom corresponding to the length of data (1958-2019, 62 years).

manuscript demonstrating that parts of the historical GrIS SMB change are attributable to AAER. Specifically, GHG drives the long-term SMB decline, while AAER contributes to the decadal variability of SMB, consistent with a growing literature on how AAER induces decadal variations to other aspects of historical North Atlantic climate change (Scaife and Smith et al., 2018).

To understand the mechanisms of forced SMB change, we consider two perspectives. First, from a mass balance perspective, we demonstrate that the historical forced SMB changes in a ERA5 reanalysis-based RACMO simulation are mainly driven by runoff changes, irrespective of the underlying forcing (GHG or AAER). Second, we investigate the atmospheric pathways by which these forcings affect runoff, demonstrating that the GHG-forced runoff change is mainly driven by long-term warming and the AAER-driven runoff change relates to atmospheric circulation variability of Greenland blocking on decadal time scales (Sherman et al., 2020; Brils et al., 2023; Hanna et al., 2022). These results highlight that different climate forcings can drive

SMB changes through different physical mechanisms, with different spatial patterns and time scales (i.e., long-term trend vs decadal variability).

295     Attribution of regional climate change to AAER often has a low S/N compared to GHG attribution (e.g., Marvel et al., 2019) and our study confirms this tendency. In the case of attributing GrIS SMB, this is due to the temperature sensitivity of runoff being weaker in AAER than GHG, as the sensitivity strongly depends on mean state temperatures in each simulation. We compare the sets of *forcing-only* (GHG and AAER) and *all-but-forcing* (xAAER and ALL-minus-xAAER) CESM2 experiments, where we show robust attribution of historical GrIS SMB changes to both GHG and AAER through runoff changes. The mean

300 state temperature dependency of runoff response can also explain the difference of S/N in the *forcing-only* and *all-but-forcing* sets, as their mean state temperatures are different. Although we show that both AAER and GHG contribute to the historical GrIS SMB changes, such a mean state temperature dependence of the forced SMB response implies a potential bias in the current D&A framework - certain forcings, such as GHG, can individually create a mean state with a stronger response that is more likely to be attributed. Future work will need to develop D&A methods than can systematically account for mean state

305 temperature dependency in climate responses.

    On top of the different runoff responses due to the mean state temperature dependence, we note that historical aerosol emissions used in CMIP6 simulations have large uncertainties, especially pre-1980 (Mahowald et al., 2024). Beyond the scope of this paper, future works should thus explore the impacts of aerosol emissions and forcing uncertainties on D&A of GrIS SMB changes.

310     The mean state temperature dependency of runoff found in our study implies that GrIS SMB changes might accelerate in the future, especially as we expect continued increases in greenhouse gases with simultaneous reductions in anthropogenic aerosols (Samset et al., 2018; Persad et al., 2022). Thus, under stronger warming in these future projections, further growth in the contribution of GrIS SMB reduction to GMSL rise is foreseeable.

*Author contributions.* All the authors were involved in the conceptualization of this project, the discussion of the interpretations of results, and the revision of the drafts. YNK analyzed the data, created the visualization, and wrote the first draft of the manuscript.

# 5   Reference

Allen, M. R. and Stott, P. A.: Estimating signal amplitudes in optimal fingerprinting, part I: theory, Climate Dynamics, 21, 477–491, https://doi.org/10.1007/s00382-003-0313-9, 2003.

325   Bamber, J. L., Westaway, R. M., Marzeion, B., and Wouters, B.: The land ice contribution to sea level during the satellite era, Environ. Res. Lett., 13, 063008, https://doi.org/10.1088/1748-9326/aac2f0, 2018.

Brils, M., Kuipers Munneke, P., and Van Den Broeke, M. R.: Spatial Response of Greenland's Firn Layer to NAO Variability, JGR Earth Surface, 128, e2023JF007082, https://doi.org/10.1029/2023JF007082, 2023.

Chen, X., Zhang, X., Church, J. A., Watson, C. S., King, M. A., Monselesan, D., Legresy, B., and Harig, C.: The increasing
330   rate of global mean sea-level rise during 1993–2014, Nature Clim Change, 7, 492–495, https://doi.org/10.1038/nclimate3325, 2017.

Church, J. A., White, N. J., Konikow, L. F., Domingues, C. M., Cogley, J. G., Rignot, E., Gregory, J. M., Van Den Broeke, M. R., Monaghan, A. J., and Velicogna, I.: Revisiting the Earth's sea-level and energy budgets from 1961 to 2008: SEA-LEVEL AND ENERGY BUDGETS, Geophys. Res. Lett., 38, n/a-n/a, https://doi.org/10.1029/2011GL048794, 2011.

335   Danabasoglu, G., Lamarque, J. -F., Bacmeister, J., Bailey, D. A., DuVivier, A. K., Edwards, J., Emmons, L. K., Fasullo, J., Garcia, R., Gettelman, A., Hannay, C., Holland, M. M., Large, W. G., Lauritzen, P. H., Lawrence, D. M., Lenaerts, J. T. M., Lindsay, K., Lipscomb, W. H., Mills, M. J., Neale, R., Oleson, K. W., Otto-Bliesner, B., Phillips, A. S., Sacks, W., Tilmes, S., Kampenhout, L., Vertenstein, M., Bertini, A., Dennis, J., Deser, C., Fischer, C., Fox-Kemper, B., Kay, J. E., Kinnison, D., Kushner, P. J., Larson, V. E., Long, M. C., Mickelson, S., Moore, J. K., Nienhouse, E., Polvani, L., Rasch, P. J., and Strand, W. G.: The
340   Community Earth System Model Version 2 (CESM2), J. Adv. Model. Earth Syst., 12, https://doi.org/10.1029/2019MS001916, 2020.

Dangendorf, S., Hendricks, N., Sun, Q., Klinck, J., Ezer, T., Frederikse, T., Calafat, F. M., Wahl, T., and Törnqvist, T. E.: Acceleration of U.S. Southeast and Gulf coast sea-level rise amplified by internal climate variability, Nat Commun, 14, 1935, https://doi.org/10.1038/s41467-023-37649-9, 2023.

345   Delhasse, A., Hanna, E., Kittel, C., and Fettweis, X.: Brief communication: CMIP6 does not suggest any atmospheric blocking increase in summer over Greenland by 2100, Intl Journal of Climatology, 41, 2589–2596, https://doi.org/10.1002/joc.6977, 2021.

Deser, C., Phillips, A. S., Simpson, I. R., Rosenbloom, N., Coleman, D., Lehner, F., Pendergrass, A. G., DiNezio, P., and Stevenson, S.: Isolating the Evolving Contributions of Anthropogenic Aerosols and Greenhouse Gases: A New CESM1 Large
350   Ensemble Community Resource, Journal of Climate, 33, 7835–7858, https://doi.org/10.1175/JCLI-D-20-0123.1, 2020a.

Deser, C., Lehner, F., Rodgers, K. B., Ault, T., Delworth, T. L., DiNezio, P. N., Fiore, A., Frankignoul, C., Fyfe, J. C., Horton, D. E., Kay, J. E., Knutti, R., Lovenduski, N. S., Marotzke, J., McKinnon, K. A., Minobe, S., Randerson, J., Screen, J. A., Simpson, I. R., and Ting, M.: Insights from Earth system model initial-condition large ensembles and future prospects, Nat. Clim. Chang., 10, 277–286, https://doi.org/10.1038/s41558-020-0731-2, 2020b.

355   Dittus, A. J., Hawkins, E., Robson, J. I., Smith, D. M., and Wilcox, L. J.: Drivers of Recent North Pacific Decadal Variability: The Role of Aerosol Forcing, Earth's Future, 9, https://doi.org/10.1029/2021EF002249, 2021.

Dong, B. and Sutton, R. T.: Recent trends in summer atmospheric circulation in the North Atlantic/European region: is there a role for anthropogenic aerosols?, Journal of Climate, 1–49, https://doi.org/10.1175/JCLI-D-20-0665.1, 2021.

Dow, W. J., Maycock, A. C., Lofverstrom, M., and Smith, C. J.: The Effect of Anthropogenic Aerosols on the Aleutian Low,
360   Journal of Climate, 34, 1725–1741, https://doi.org/10.1175/JCLI-D-20-0423.1, 2021.

Enderlin, E. M., Howat, I. M., Jeong, S., Noh, M., Van Angelen, J. H., and Van Den Broeke, M. R.: An improved mass budget for the Greenland ice sheet, Geophysical Research Letters, 41, 866–872, https://doi.org/10.1002/2013GL059010, 2014.

Frederikse, T., Landerer, F., Caron, L., Adhikari, S., Parkes, D., Humphrey, V. W., Dangendorf, S., Hogarth, P., Zanna, L., Cheng, L., and Wu, Y.-H.: The causes of sea-level rise since 1900, Nature, 584, 393–397, https://doi.org/10.1038/s41586-020-
365   2591-3, 2020.

Gottlieb, A. R. and Mankin, J. S.: Evidence of human influence on Northern Hemisphere snow loss, Nature, 625, 293–300, https://doi.org/10.1038/s41586-023-06794-y, 2024.

Hanna, E., Fettweis, X., Mernild, S. H., Cappelen, J., Ribergaard, M. H., Shuman, C. A., Steffen, K., Wood, L., and Mote, T. L.: Atmospheric and oceanic climate forcing of the exceptional Greenland ice sheet surface melt in summer 2012, Intl Journal
370   of Climatology, 34, 1022–1037, https://doi.org/10.1002/joc.3743, 2014.

Hanna, E., Cropper, T. E., Hall, R. J., Cornes, R. C., and Barriendos, M.: Extended North Atlantic Oscillation and Greenland Blocking Indices 1800–2020 from New Meteorological Reanalysis, Atmosphere, 13, 436, https://doi.org/10.3390/atmos13030436, 2022.

Hay, C. C., Morrow, E., Kopp, R. E., and Mitrovica, J. X.: Probabilistic reanalysis of twentieth-century sea-level rise, Nature,
375   517, 481–484, https://doi.org/10.1038/nature14093, 2015.

He, C., Clement, A. C., Kramer, S. M., Cane, M. A., Klavans, J. M., Fenske, T. M., and Murphy, L. N.: Tropical Atlantic multidecadal variability is dominated by external forcing, Nature, 622, 521–527, https://doi.org/10.1038/s41586-023-06489-4, 2023.

Hersbach, H., Bell, B., Berrisford, P., Hirahara, S., Horányi, A., Muñoz-Sabater, J., Nicolas, J., Peubey, C., Radu, R., Schep-
380   ers, D., Simmons, A., Soci, C., Abdalla, S., Abellan, X., Balsamo, G., Bechtold, P., Biavati, G., Bidlot, J., Bonavita, M., Chiara, G., Dahlgren, P., Dee, D., Diamantakis, M., Dragani, R., Flemming, J., Forbes, R., Fuentes, M., Geer, A., Haimberger, L., Healy, S., Hogan, R. J., Hólm, E., Janisková, M., Keeley, S., Laloyaux, P., Lopez, P., Lupu, C., Radnoti, G., Rosnay, P., Rozum, I., Vamborg, F., Villaume, S., and Thépaut, J.: The ERA5 global reanalysis, Q.J.R. Meteorol. Soc., 146, 1999–2049, https://doi.org/10.1002/qj.3803, 2020.

385   Hofer, S., Lang, C., Amory, C., Kittel, C., Delhasse, A., Tedstone, A., and Fettweis, X.: Greater Greenland Ice Sheet contribution to global sea level rise in CMIP6, Nat Commun, 11, 6289, https://doi.org/10.1038/s41467-020-20011-8, 2020.

Hwang, Y.-T., Xie, S.-P., Chen, P.-J., Tseng, H.-Y., and Deser, C.: Contribution of anthropogenic aerosols to persistent La Niña-like conditions in the early 21st century, Proc. Natl. Acad. Sci. U.S.A., 121, e2315124121, https://doi.org/10.1073/pnas.2315124121, 2024.

390    IPCC, 2023: Climate Change 2023: Synthesis Report. Contribution of Working Groups I, II and III to the Sixth Assessment
       Report of the Intergovernmental Panel on Climate Change [Core Writing Team, H. Lee and J. Romero (eds.)]. IPCC, Geneva,
       Switzerland, pp. 35-115, doi: 10.59327/IPCC/AR6-9789291691647.

       Kang, J. M., Shaw, T. A., and Sun, L.: Anthropogenic Aerosols Have Significantly Weakened the Regional Summertime Cir-
       culation in the Northern Hemisphere During the Satellite Era, AGU Advances, 5, e2024AV001318, https://doi.org/10.1029/2024AV001318,
395    2024.

       Katzfuss, M., Hammerling, D., and Smith, R. L.: A Bayesian hierarchical model for climate change detection and attribution,
       Geophysical Research Letters, 44, 5720–5728, https://doi.org/10.1002/2017GL073688, 2017.

       Kirchmeier-Young, M. C., Zwiers, F. W., and Gillett, N. P.: Attribution of Extreme Events in Arctic Sea Ice Extent, Journal
       of Climate, 30, 553–571, https://doi.org/10.1175/JCLI-D-16-0412.1, 2017.

400    Kjeldsen, K. K., Korsgaard, N. J., Bjørk, A. A., Khan, S. A., Box, J. E., Funder, S., Larsen, N. K., Bamber, J. L., Colgan,
       W., Van Den Broeke, M., Siggaard-Andersen, M.-L., Nuth, C., Schomacker, A., Andresen, C. S., Willerslev, E., and Kjær,
       K. H.: Spatial and temporal distribution of mass loss from the Greenland Ice Sheet since AD 1900, Nature, 528, 396–400,
       https://doi.org/10.1038/nature16183, 2015.

       Kuo, Y., Kim, H., and Lehner, F.: Anthropogenic Aerosols Contribute to the Recent Decline in Precipitation Over the U.S.
405    Southwest, Geophysical Research Letters, 50, e2023GL105389, https://doi.org/10.1029/2023GL105389, 2023.

       Kuo, Y.-N., Lehner, F., Simpson, I. R., Deser, C., Phillips, A. S., Newman, M., Shin, S.-I., Wong, S., and Arblaster, J.
       M.: Recent southwestern US drought exacerbated by anthropogenic aerosols and tropical ocean warming, Nat. Geosci., 18,
       578–585, https://doi.org/10.1038/s41561-025-01728-x, 2025.

       Lipscomb, W. H., Price, S. F., Hoffman, M. J., Leguy, G. R., Bennett, A. R., Bradley, S. L., Evans, K. J., Fyke, J. G., Kennedy,
410    J. H., Perego, M., Ranken, D. M., Sacks, W. J., Salinger, A. G., Vargo, L. J., and Worley, P. H.: Description and evaluation of
       the Community Ice Sheet Model (CISM) v2.1, Geosci. Model Dev., 12, 387–424, https://doi.org/10.5194/gmd-12-387-2019,
       2019.

       Mahowald, N. M., Li, L., Albani, S., Hamilton, D. S., and Kok, J. F.: Opinion: The importance of historical and paleoclimate
       aerosol radiative effects, Atmos. Chem. Phys., 24, 533–551, https://doi.org/10.5194/acp-24-533-2024, 2024.

415    Marvel, K., Cook, B. I., Bonfils, C. J. W., Durack, P. J., Smerdon, J. E., and Williams, A. P.: Twentieth-century hydroclimate
       changes consistent with human influence, Nature, 569, 59–65, https://doi.org/10.1038/s41586-019-1149-8, 2019.

       McKenna, C. M. and Maycock, A. C.: Sources of Uncertainty in Multimodel Large Ensemble Projections of the Winter North
       Atlantic Oscillation, Geophysical Research Letters, 48, e2021GL093258, https://doi.org/10.1029/2021GL093258, 2021.

       McKitrick, R.: On the choice of TLS versus OLS in climate signal detection regression, Clim Dyn, 60, 359–374, https://doi.org/10.1007/s00382-
420    022-06315-z, 2023.

       Mitrovica, J. X., Tamisiea, M. E., Davis, J. L., and Milne, G. A.: Recent mass balance of polar ice sheets inferred from
       patterns of global sea-level change, Nature, 409, 1026–1029, https://doi.org/10.1038/35059054, 2001.

Mouginot, J., Rignot, E., Bjørk, A. A., Van Den Broeke, M., Millan, R., Morlighem, M., Noël, B., Scheuchl, B., and Wood, M.: Forty-six years of Greenland Ice Sheet mass balance from 1972 to 2018, Proc. Natl. Acad. Sci. U.S.A., 116, 9239–9244, 425 https://doi.org/10.1073/pnas.1904242116, 2019.

Noël, B., Van De Berg, W. J., Van Wessem, J. M., Van Meijgaard, E., Van As, D., Lenaerts, J. T. M., Lhermitte, S., Kuipers Munneke, P., Smeets, C. J. P. P., Van Ulft, L. H., Van De Wal, R. S. W., and Van Den Broeke, M. R.: Modelling the climate and surface mass balance of polar ice sheets using RACMO2 – Part 1: Greenland (1958–2016), The Cryosphere, 12, 811–831, https://doi.org/10.5194/tc-12-811-2018, 2018.

430 Noël, B., Van De Berg, W. J., Lhermitte, S., and Van Den Broeke, M. R.: Rapid ablation zone expansion amplifies north Greenland mass loss, Sci. Adv., 5, eaaw0123, https://doi.org/10.1126/sciadv.aaw0123, 2019.

Noël, B., Van Kampenhout, L., Van De Berg, W. J., Lenaerts, J. T. M., Wouters, B., and Van Den Broeke, M. R.: Brief communication: CESM2 climate forcing (1950–2014) yields realistic Greenland ice sheet surface mass balance, The Cryosphere, 14, 1425–1435, https://doi.org/10.5194/tc-14-1425-2020, 2020.

435 Noël, B., Lenaerts, J. T. M., Lipscomb, W. H., Thayer-Calder, K., and Van Den Broeke, M. R.: Peak refreezing in the Greenland firn layer under future warming scenarios, Nat Commun, 13, 6870, https://doi.org/10.1038/s41467-022-34524-x, 2022.

Oudar, T., Kushner, P. J., Fyfe, J. C., and Sigmond, M.: No Impact of Anthropogenic Aerosols on Early 21st Century Global Temperature Trends in a Large Initial-Condition Ensemble, Geophys. Res. Lett., 45, 9245–9252, https://doi.org/10.1029/2018GL078841, 440 2018.

Pattyn, F., Ritz, C., Hanna, E., Asay-Davis, X., DeConto, R., Durand, G., Favier, L., Fettweis, X., Goelzer, H., Golledge, N. R., Kuipers Munneke, P., Lenaerts, J. T. M., Nowicki, S., Payne, A. J., Robinson, A., Seroussi, H., Trusel, L. D., and Van Den Broeke, M.: The Greenland and Antarctic ice sheets under 1.5 °C global warming, Nature Clim Change, 8, 1053–1061, https://doi.org/10.1038/s41558-018-0305-8, 2018.

445 Persad, G. G., Samset, B. H., and Wilcox, L. J.: Aerosols must be part of climate risk assessments, 2022.

Rodgers, K. B., Lee, S.-S., Rosenbloom, N., Timmermann, A., Danabasoglu, G., Deser, C., Edwards, J., Kim, J.-E., Simpson, I. R., Stein, K., Stuecker, M. F., Yamaguchi, R., Bódai, T., Chung, E.-S., Huang, L., Kim, W. M., Lamarque, J.-F., Lombardozzi, D. L., Wieder, W. R., and Yeager, S. G.: Ubiquity of human-induced changes in climate variability, Earth Syst. Dynam., 12, 1393–1411, https://doi.org/10.5194/esd-12-1393-2021, 2021.

450 Samset, B. H., Sand, M., Smith, C. J., Bauer, S. E., Forster, P. M., Fuglestvedt, J. S., Osprey, S., and Schleussner, C. -F.: Climate Impacts From a Removal of Anthropogenic Aerosol Emissions, Geophysical Research Letters, 45, 1020–1029, https://doi.org/10.1002/2017GL076079, 2018.

Scaife, A. A. and Smith, D.: A signal-to-noise paradox in climate science, npj Clim Atmos Sci, 1, 28, https://doi.org/10.1038/s41612-018-0038-4, 2018.

455 Schurer, A. P., Hegerl, G. C., Mann, M. E., Tett, S. F. B., and Phipps, S. J.: Separating Forced from Chaotic Climate Variability over the Past Millennium, Journal of Climate, 26, 6954–6973, https://doi.org/10.1175/JCLI-D-12-00826.1, 2013.

Sherman, P., Tziperman, E., Deser, C., and McElroy, M.: Historical and Future Roles of Internal Atmospheric Variability in Modulating Summertime Greenland Ice Sheet Melt, Geophysical Research Letters, 47, e2019GL086913, https://doi.org/10.1029/2019GL086913, 2020.

460     Simpson, I. R., Rosenbloom, N., Danabasoglu, G., Deser, C., Yeager, S. G., McCluskey, C. S., Yamaguchi, R., Lamarque, J.-F., Tilmes, S., Mills, M. J., and Rodgers, K. B.: The CESM2 Single-Forcing Large Ensemble and Comparison to CESM1: Implications for Experimental Design, Journal of Climate, 36, 5687–5711, https://doi.org/10.1175/JCLI-D-22-0666.1, 2023.

Swart, N. C., Gille, S. T., Fyfe, J. C., and Gillett, N. P.: Recent Southern Ocean warming and freshening driven by greenhouse gas emissions and ozone depletion, Nature Geosci, 11, 836–841, https://doi.org/10.1038/s41561-018-0226-1, 2018.

465     Takahashi, C. and Watanabe, M.: Pacific trade winds accelerated by aerosol forcing over the past two decades, Nature Clim Change, 6, 768–772, https://doi.org/10.1038/nclimate2996, 2016.

Tedesco, M. and Fettweis, X.: Unprecedented atmospheric conditions (1948–2019) drive the 2019 exceptional melting season over the Greenland ice sheet, The Cryosphere, 14, 1209–1223, https://doi.org/10.5194/tc-14-1209-2020, 2020.

Thompson-Munson, M., Kay, J. E., and Markle, B. R.: Greenland's firn responds more to warming than to cooling, The 470   Cryosphere, 18, 3333–3350, https://doi.org/10.5194/tc-18-3333-2024, 2024.

Trusel, L. D., Das, S. B., Osman, M. B., Evans, M. J., Smith, B. E., Fettweis, X., McConnell, J. R., Noël, B. P. Y., and Van Den Broeke, M. R.: Nonlinear rise in Greenland runoff in response to post-industrial Arctic warming, Nature, 564, 104–108, https://doi.org/10.1038/s41586-018-0752-4, 2018.

van Kampenhout, L., Lenaerts, J. T. M., Lipscomb, W. H., Lhermitte, S., Noël, B., Vizcaíno, M., Sacks, W. J., and van 475   den Broeke, M. R.: Present-Day Greenland Ice Sheet Climate and Surface Mass Balance in CESM2, JGR Earth Surface, 125, e2019JF005318, https://doi.org/10.1029/2019JF005318, 2020.

Wdowinski, S., Bray, R., Kirtman, B. P., and Wu, Z.: Increasing flooding hazard in coastal communities due to rising sea level: Case study of Miami Beach, Florida, Ocean & Coastal Management, 126, 1–8, https://doi.org/10.1016/j.ocecoaman.2016.03.002, 2016.

480     Wu, Y., Liang, Y., Kuo, Y., Lehner, F., Previdi, M., Polvani, L. M., Lo, M., and Lan, C.: Exploiting SMILEs and the CMIP5 Archive to Understand Arctic Climate Change Seasonality and Uncertainty, Geophysical Research Letters, 50, e2022GL100745, https://doi.org/10.1029/2022GL100745, 2023.